Physico-chemical characterisation of plant particles with potential to produce biobased building materials

Santiago Arufe, Arthur Hellouin de Menibus, Nathalie Leblanc, Hélène Lenormand

Physico-chemical characterisation of plant particles with potential to produce biobased building materials

Santiago Arufe[a*], Arthur Hellouin de Menibus[b,c], Nathalie Leblanc[a], Hélène Lenormand[a]

[a]UniLaSalle, Univ. Artois, ULR7519 - Transformations & Agro-ressources, Normandie Université, F-76130 Mont Saint Aignan, France

[b]Eco-Pertica, L'Hôtel Buissonnet, 61340 Nocé, France

[c]French National Association of Short Distribution Network Hemp Producers (Association Nationale des Chanvriers en Circuits Courts), France

*Corresponding Author: santiago.arufe@gmail.com

Abstract

A physico-chemical characterisation of flax shiv (*Linum usitatissimum*), hemp shiv (*Cannabis sativa L.*), maize bark (*Zea mays L.*), miscanthus (*Miscanthus*), reed (*Phragmites australis*), rice husk (*Oryza sativa*), sunflower (*Helianthus annuus*) bark and pith and wheat (*Triticum*) by means of chemical composition, particle size, density and water behaviour was carried out in order to facilitate their comparison. Particle size distribution, water sorption isotherms and water absorption kinetics of the plant particles were modelled using respectively the log-normal distribution, GAB and Nagy and Vas models. Results of chemical composition (soluble compounds 6.0-38.6 g/100 g dry material (% d.b.), hemicellulose: 5.0-34.8 % d.b., cellulose: 23.3-49.0 % d.b., lignin: 3.3-41.7 % d.b., ashes: 2.4-13.7 % d.b.) highlight the heterogeneity of the studied materials. Sunflower bark showed the largest mean values for length (10.7 mm) and width (3.9 mm) hemp shiv being the smallest studied particle with 4.5 mm of length and 1.2 mm of width. The range of values of bulk density for the studied samples varied from 21 kg/m^3 (sunflower pith) up to 157 kg/m^3 (sunflower bark). A slight linear relationship (R^2<0.87) was found between porosity and bulk density of plant particles.

Water absorption kinetics were consistent with the plant chemical composition and the open porosity which highlight a fair understanding of inter-dependence of particles physical properties.

Keywords: density; porosity; sorption; bio-based aggregate; building material

1. Introduction

The renovation and construction of buildings reducing the global warming potential can be partly addressed by using low-environmental-impact materials such as raw biobased materials. In France, hemp and straw are the most well-known plants used for building applications (Colinart et al., 2020), hemp crop represented 17000 ha in 2018 (FAOSTAT) and it generated about 50000 t of hemp shiv. Hemp production can be increased due to its usefulness for farmers that goes toward low impact agriculture schemes. A way to enhance the sustainability could be diversify the use of different biobased particles in construction rather than the use of only one kind of plant particle. Firstly, this may allow the use of plant particles available at local scale. Secondly, it could reduce the risk of competition with other ways for the valorisation of the same plant particles (litter, bioenergy, etc). Laborel et al. (2016) in their review about earth construction highlighted the great diversity of bio-aggregates (plant and animal) used worldwide. This review identified cereal straws (wheat, barley, oat, lavender (Giroudon et al., 2019)), wood aggregates (shavings or fibres), bast fibres (hemp, flax, jute, kenaf, diss), palm tree fibres (coir, palm, date), wastes and residues (cassava, millet, cotton, tea, tobacco, grass), leaf fibres (sisal, banana, pineapple), aquatic plants (phragmite, typha, seaweed) and wool (sheep). Jiang et al. (2020) specifically characterized hemp shiv, flax shiv, rape shiv and wheat straw as hygric and insulating construction materials for energy efficient building. Other works assessed the use of maize or sunflower bark chips (Lagouin et al., 2019), reed (Honoré et al., 2020), miscanthus (Ntimugura et al., 2020) and rice/rice husk ash (Taye et al., 2021) for bio-based building materials. In France, the main crops able to produce particles with potential applications in

55 construction are cereals (wheat, barley, oat, rye, rice), oil plants (sunflower, rapeseed),
56 herbaceous plants (corn, miscanthus, reed) and fibre plants (flax, hemp).
57 Microstructure and biochemistry are two of the important parameters to be studied in order to
58 understand how plant particles would behave when used as a building material. The
59 microstructure of plant particles can be studied at different scales (Glé et al., 2021). The bulk
60 density, which is characterized by the mass of the particles per volume unit, gives the overall
61 density of the bulk plant material. It is calculated by measuring the total volume occupied by a
62 certain mass of plant particles. The total volume is the result of the sum of different volumes:
63 a) the volume occupied by the walls of the particles; b) the volume of air between the particles
64 and c) the volume of occupied air inside the particles. The volume occupied by the walls of
65 the particles (a) could be considered intrinsic of the material. The air-filled volume between
66 the particles (b) is dependent on the arrangement of the particles between them which is
67 influenced by their shape and particle size. Therefore, this volume may be decreased by
68 grinding or milling which could have a positive effect on the arrangement between the
69 particles and as a consequence increase the apparent density. Finally, c) includes the volume
70 accessible from the outside of the particle (open porosity) and the volume not accessible
71 (closed porosity) (Delannoy et al., 2020).
72 Functionalities are properties induced by the intrinsic characteristics of plant particles. These
73 characteristics such as the microstructure, chemical composition or water behaviour may lead
74 to functionalities that can be positive or negative depending on the final use of the plant
75 particle. A clear example of a functionality related to chemical composition that can be
76 positive or negative as function of the final use is the search for ecological solutions in the
77 design of particleboard. By using the self-adhesion capacity, it is possible to process particle
78 boards without the addition of binders, thanks to the action of different parameters such as
79 solubilization of molecules, temperature and pressure which allow the particles to
80 agglomerate with each other (Lenormand et al., 2017, Pintiaux et al., 2015). However, this
81 ability to solubilize molecules could be considered a negative functionality when the

molecules disturb the setting of lime or cement-based mortars (Diquélou et al., 2015; Wang et al., 2019).

The cell walls of plant particles are mainly composed of a mix of organic macromolecules (pectins, cellulose, hemicelluloses, lignin, waxes, starch, proteins, aromatic compounds, short-chain sugars) and a minority of mineral molecules such as ashes. Cell walls can therefore be considered as biochemically complex composites. Cellulose molecules, hemicelluloses and pectins are polysaccharides (polymers of carbohydrates) with hydrophilic properties. The water-soluble compounds generally correspond to pectins and short-chained soluble molecules. The proportions of organic macromolecules vary according to the botanical species and the location in the plant. For example, sunflower pith stands out from the others with a proportion of water-soluble compounds higher than 50% (Chabriac et al., 2016).

In order to clear out what are the essential differences between these plant particles, a physico-chemical characterization with the same techniques and protocols in order to facilitate the comparison was carried out. The procedure was applied to 9 different plant particles that can be obtained in France, focusing on the particle size, the hygroscopic behaviour, the chemical composition, the densities and the water absorption behaviour.

2. Materials and Methods

2.1. Materials

Nine different plant particles were studied: A) flax (*Linum usitatissimum*) shiv bought on a local market, Linabox (76590 Crosville sur Scie, France); B) hemp (*Cannabis sativa L.*) shiv bought in a local market and produced in France; C) maize (*Zea mays L.*) bark particles obtained from stems of maize cultivated in Villainville (Seine-Maritime, France) in 2015; D) miscanthus (*Miscanthus*) particles obtained on a local market, Miscanplus (28250 Digny, France); E) reed (*Phragmites australis*) particles obtained after milling and sieving (the studied fraction corresponded to particles that were retained between 2 and 8 mm sieves) of reed from the Brenne region (Centre-Val de Loire, France); F) rice (*Oryza sativa*) husk,

obtained from a high density batch (Balle Concept, 13200 Arles, France) that was sieved with a sieve of 10 mm, vacuuming once to remove heavy parts (grains and others) and re-sieved with a sieve of 10 mm; G) sunflower *(Helianthus annuus)* bark and sunflower pith (H) obtained from sunflower stem kindly provided by the farm cooperative *Oxyane* and I) wheat (*Triticum*) particles obtained from wheat cultivated in Normandie in 2017.

The employed hemp and flax shiv were obtained by raw plant transformation by a large scale defibrator plant that was hammer milled during the defibrating process. Maize bark and wheat studied particles were obtained after milling employing a cutting mill (Retsch SM100, Germany) equipped with a standard sieve with 10 mm of mesh size. All different samples were sieved employing a standard sieve of 0.5 mm in order to eliminate dust that could have influence on the subsequent studies.

Location of Figure 1

2.2. Chemical Composition

Chemical composition of samples, content of ash, lignin, cellulose, hemicellulose and soluble compounds in neutral detergent was determined following the Van Soest method (AFNOR, 1997, Viel et al., 2018) employing an adapted machine (FibertcTR 8000, Foss, Denmark). To carry out this measurement all samples were previously dried until constant weight at 40ºC using an oven (Memmert, Germany) and then milled employing a micro impact mill (Culatti, Switzerland), the rotor speed was adjusted to 7 and a standard sieve of 1 mm of mesh size was employed. All measurements were carried out at least in triplicate.

2.3. Particle size characterization

Particle size distribution of all samples was determined by image analysis employing the protocol described by Amziane & Collet (2017) slightly modified. Images of each sample were taken employing a vision system (Keyence, CA-MX500M) placing their particles on a plate (CA-DSW15) where a maximum of 200 particles were placed to take the photos. Size of

particles was then determined employing a scale factor of 0.0609 mm/pixel employing the associated software of the machine. At least 1000 particles of each sample were measured. Experimental data was modelled employing the error function in order to confirm if this function can be a good model to predict experimental particle size distribution of samples. The model is defined as, Eq. (1):

$$P = \frac{1}{2}\left(1 + erf\left(\frac{\ln(x)-\mu}{\sqrt{2}\sigma}\right)\right) \quad (1)$$

where P is the cumulative frequency, erf the error function ($\mathrm{erf}(z) = \frac{2}{\sqrt{\pi}}\int_0^z e^{-t^2} dt$), x the variable (in this case width or length) and μ and σ are model parameters corresponding to mean and standard deviation of the variable's natural logarithm.

2.4. Bulk and true density

2.4.1. Bulk Density

Two different bulk densities of samples previously dried at 40ºC until constant weight were calculated employing different methods: apparent and compacted density. Apparent density (ρ_A) was calculated by measuring the height of a known quantity of sample placed in a cylinder that was upended ten times (Amziane & Collet 2017). For compacted density (ρ_C) a known quantity of samples was placed in a cylinder then it was manually compressed and finally the volume of the sample was determined (Glé et al., 2021). All measurements were carried out at least in triplicate.

2.4.2. True Density

True density (ρ_T) of samples was calculated after measurement of sample volume by gas displacement using a gas pycnometer (Pycnomatic Evo, ThermoScientific) with argon as employed gas. The gas was introduced into a small vessel (21.42 cm^3) at a constant temperature of 23ºC where the sample was previously placed. The pressure (P) was set at 1

bar (with highest and lowest limit of 1.5 bar and 0.5 bar, respectively) considering that sample is in equilibrium when ΔP between different measurements is lower than 0.00020 bar and volume standard deviation lower than 0.050 %. True density was then calculated by ratio of sample mass (previously determined) and sample volume determined by gas displacement. Each sample was measured at least in duplicate.

Once both true and apparent density were obtained, open porosity was calculated as follows, Eq. (2):

$$\theta_{open} = 1 - \frac{\rho_A}{\rho_T} \quad (2)$$

where θ_{open} corresponded to open porosity (-) and ρ_A and ρ_T to, respectively, apparent and true density (kg/m^3) of samples determined as previously explained.

2.5. Water sorption isotherms

Water sorption isotherms of samples were determined at 23ºC using a Dynamic Vapour Sorption machine (SPS-Sorption Test System, proUmid), employing nitrogen as gas in order to control relative humidity (φ). At least duplicate samples (219±34 mg as average sample weight) were measured. Different equilibrium points were determined corresponding to a fixed relative humidity: 0, 5, 10, 15, 20, 30, 35, 50, 75, 85 and 90 % for adsorption experiments, and 0, 15, 30, 35, 50, 75, 85, 90 % for desorption experiments. Samples employed for adsorption experiments were previously air-dried until constant weight in an oven (Memmert, Germany) at 40ºC. Desorption samples were previously exposed to a relative humidity of 90% for hydration until they reached a constant weight.

GAB (van den Berg & Bruin (1981), Eq. (3)) and BET models (Brunauer *et al.*, 1938, Eq. (4)) were employed to model water sorption experimental data (equilibrium moisture content, X_{eq} *versus* φ):

$$X_{eq} = \frac{X_m K C \phi}{(1-K\phi)(1-K\phi+CK\phi)} \quad (3)$$

$$X_{eq} = \frac{X_m C \phi}{(1-\phi)(1+(C-1)\phi)} \quad (4)$$

where X_m is the monolayer moisture content (kg water/kg dried solid, dry basis: d.b.), C (dimensionless, -) and K (dimensionless, -) is a parameter related to the heat of sorption of the multilayer in GAB model. The values of GAB model parameters give different information. C parameter is related to the water bound in the monolayer, the higher C, the stronger water is bound in the monolayer and the higher the difference in enthalpy between the monolayer molecules and multilayer molecules (Quirijns et al., 2015). K is called a correction factor, since it corrects the properties of the multilayer molecules relative to the bulk liquid. When K approaches one, there is almost no distinction between multilayer molecules and liquid molecules. In that case the water molecules beyond the monolayer are not structured in a multilayer, but have the same characteristics as the molecules in the bulk liquid. The more the sorbed molecules are structured in a multilayer, the lower the value for K (Quirijns et al., 2015). Finally, X_m is a measure of the availability of active sites for water sorption by the material. It has to be noted that BET was applied in the range of relative humidity from 0.05 to 0.35 in order to determine the specific surface area of samples (Collet *et al.*, (2008)) assuming that X_m of BET model represents the quantity of water molecules that covers the entire surface as a monolayer and no diffusion of water through the material has taken place. Experimental data was modelled using these two methods employing Solver function of Excel software. In the case of BET model, once model parameters were obtained, specific surface area was calculated as follows, Eq. (5):

$$a_s = \frac{X_m L a_m}{M_w} \quad (5)$$

where a_s is the specific surface area of the sample (m^2/g), L the Avogadro constant ($6.023 \cdot 10^{23}$ mol^{-1}), a_m cross sectional area of water molecule ($1.08 \cdot 10^{-19}$ m^2) and M_w molecular weight of water molecules (18 g/mol).

2.6. Water absorption kinetics

Water absorption kinetics of different samples were determined at 5, 15, 60, 480, 1440, 2880 min (t) employing a protocol based on the one previously published by Amziane & Collet (2017) with some modifications. Samples ($M_0 \approx 1$ g) previously dried at 40ºC until constant weight using an oven (Memmert, Germany) were put in a water bath (water temperature 23.0±0.5ºC) during different periods of time employing a tea strainer ball. Once the desired time of immersion was achieved, samples were removed and filtered by vacuum filtration with a Büchner funnel using a paper filter, in order to eliminate the excess of water on the surface of the material, and finally weighed to determine the mass of the sample after immersion (M_t, g). Afterwards, samples were dried in an oven (Memmert, Germany) at 105ºC until constant weight ($M_{105ºC}$, g). Each experimental data point of water absorption kinetics were carried out at least in triplicate.

In order to analyse the water absorption kinetics different parameters were calculated: water absorption related to initial dry mass (WA_{M0}, kg water/kg initial dry mass, Eq. (6)); water absorption related to final dry mass (WA_{Mf}, kg water/kg final dry mass, Eq. (7), which takes into account the mass lost due to leaching during immersion) and solid loss during immersion (SL, kg lost dry solid/kg final dry mass, Eq. (8)):

$$WA_{M_0} = \frac{M_t}{M_0} \quad (6)$$

$$WA_{M_f} = \frac{M_t}{M_{105ºC}} \quad (7)$$

$$SL = \frac{M_0 - M_{105ºC}}{M_{105ºC}} \quad (8)$$

These parameters were finally modelled employing a function developed by Nagy and Vas (Nagy and Vas 2003) that gives an asymptotically correct approximation of the capillary water uptake process for both t→0 and t→∞, Eq. (9):

$$\Delta m(t) = \Delta m_{\infty}(1 - e^{-At^{\frac{1}{2}B}})^{B} \quad (9)$$

where A and B are constant parameters, Δm_{∞} is the modelled parameter related to equilibrium (when t→∞) and Δm(t) is the experimental data of water absorption kinetics (WA_{M0}, WA_{MF} or SL).

2.7. Scanning electro microscopy (SEM)

Images of samples were taken employing scanning electro microscopy (JSM-IT100 LA, JEOL, Japan) under vacuum conditions (40 Pa) and an accelerating voltage of 15 kV.

2.8. Statistical analysis

The goodness of the adjustment of each model was determined based on coefficient of determination (R^2) and root mean square error (E_{RMS}, Eq. (10)):

$$E_{RMS} = [\frac{1}{N}\sum_{i=1}^{i=N} (X_{\exp} - X_{cal})^2]^{1/2} \quad (10)$$

where N is the number of data points, X_{exp} the experimental data point and X_{cal} the calculated data point using the corresponding model. The values of the parameters of each model were obtained with an automated least square minimization approach.

3. Results and Discussion

3.1. Chemical Composition

Table 1 highlights the heterogeneity of the studied materials. In the case of soluble compounds, the range values varied from 6.0 up to 38.6 % d.b., sunflower pith had the highest value whereas sunflower bark presented the lowest one. Most of the studied samples presented values of soluble compounds around 10 % d.b.. Hemicellulose ranged between 5.0 to 34.8 % d.b and in most of the studied samples it was the second most important fraction on the materials composition. Cellulose is the main component of all studied samples except for sunflower bark and pith where the highest percentage corresponded respectively to lignin and soluble compounds. The cellulose values varied from 23.3 to 49.0 % d.b.. Lignin represented between 3.3 to 41.7 % d.b.. Finally, ashes varied from 2.4 % for miscanthus to 13.7 % d.b. for rice husk. Except for sunflower pith and rice husk, the percentage of ashes on the studied samples always represented the smallest part of their composition.

The composition of the different studied plant particles was similar of the one previously published in literature by different authors even if in certain cases the comparison is difficult due to the use of different methods. Flax shiv (Mahieu et al., 2019), hemp shiv (Viel et al., 2018), maize bark (Zhang et al., 2018), miscanthus (Ntimugura et al., 2020), reed (Honoré et al., 2020), rice husk (Chandrasekhar et al., 2003), sunflower bark and pith (Chabriac et al., 2016) and wheat (Viel et al., 2018).

For a specific plant, its chemical composition may vary as function of the geography, the weather and the maturity of the plant (Viel et al., 2018). The botanical species and the location in the plant can also influence the chemical composition. In this sense, the difference on chemical composition between sunflower bark and pith could be explained by their location. Sunflower bark, which is obtained from outer part of the stem (mainly responsible of the structural stability of the plant), had a higher proportion of hemicellulose, cellulose and lignin because they are polymers with a very important supportive structural function. On the other hand sunflower pith, obtained from the inner part of the stem where the structural function is less important, presented a lower proportion of these polymers and a higher

proportion of non-structural components (soluble compounds). Hemp and flax shiv show similar compositions (mainly composed of cellulose), which may also be linked to the fact that they are obtained from the same location of the plant stem. Chemical composition of wheat particles and maize bark particles are similar, with high contents of hemicellulose and cellulose, and intermediate contents of soluble compounds. For miscanthus and reed particles chemical composition is similar, with high contents of hemicellulose and cellulose, and low contents of soluble compounds. Compositions of sunflower pith, sunflower bark and rice husk particles differ from all others with, respectively, high content of soluble, lignin and ash.

Location of Table 1

3.2. Particle size characterization, density and porosity

Particle size characterization of different samples showed that most of them can be satisfactorily fitted employing a lognormal model for both length and width parameters (R^2>0.993 and E_{RMS}<0.027). The exception corresponded to rice husk length where the lognormal model was unable to fit rice husk length, particularly at lower sizes, Table 2. Taking into account that the selected plant particles may come from different parts of the plant: 1) the inner part of the stem (flax shiv, hemp shiv, sunflower and maize pith); 2) the outer part of the stem (sunflower and maize bark); 3) the whole stem (fragments of the stems obtained after grinding: wheat or miscanthus) or 4) the husks (envelopes) of grains of rice and the differences in terms of shape and texture could be remarkable, from elongated and rigid (*i.e.* sunflower bark, miscanthus) to thin and deformable (*i.e.* flax shiv, wheat or reed) or spherical/cubic and sponge-like (i.e. sunflower pith particles) the use of the same model to manage their particle size distribution may prove to be useful. Largest and smallest particles for both length and width were the same: sunflower bark showed the largest mean values (10.7 mm for length and 3.9 for width) hemp shiv being the smallest studied particle with a mean value of 4.5 mm for length and 1.2 mm for width. Several particles were ground up

and/or sieved during the transformation process, so the particle size distribution is not an intrinsic property of plant particles.

Regarding density values, it has been found that in the case of bulk density sunflower bark showed the highest value followed by miscanthus, hemp shiv, rice husk and flax shiv, Table 2. The lowest values corresponded to sunflower pith, wheat, maize bark and reed. The range of values for the studied samples varied between 21 kg/m^3 and 157 kg/m^{3,} which is the result of differences between intrinsic properties of each material and of the grinding and/or sieving process. These values are in accordance with those previously published by Chabriac et al. (2016), which studied hemp shiv, sunflower bark and pith, flax shiv and rapeseed.

Location of Table 2

In the case of true density, sunflower pith was also the material with the lowest density. However, it was observed that for the other studied samples, true density did not follow the same trend of bulk density. For example, flax shiv and sunflower bark presented the highest true density whereas they showed intermediate bulk densities. This fact reflects that bulk density can be influenced by other properties of the material such as particle size and shape that could lead to different arrangement of the material in the bulk. Specifically, in the case of sunflower bark this difference can be related to the higher particle size in the bulk which could lead to an arrangement in the bulk with higher void volume leading to a lower bulk density. In this sense, this is corroborated by the higher porosity obtained for this material. Even if grinding and sieving processes affect the particle shape and arrangement, a slight linear relationship (R^2<0.87) between the porosity and the bulk density was found: the higher the porosity, the lower the bulk density. Figure 1, shows as a qualitative example, the different microstructures of each plant particle obtained employing SEM.

3.3. Water sorption isotherms

Water adsorption-desorption isotherms of all studied samples were satisfactorily modelled employing GAB model (Eq. 3) (R^2>0.9994; E_{RMS}<0.003; Table 3) which confirms the type II isotherm (Collet et al., 2008), Figure 2a and 2b.

Location of Table 3 and Figure 2

At high relative humidities (>0.80), three main groups of plant particles could be established. Sunflower pith, maize bark and hemp shiv presented equilibrium moisture contents >0.24 kg water/kg initial dry solid; wheat and sunflower bark showed X_{eq} between 0.20 and 0.22 and rice husk, miscanthus, reed and flax shiv were the ones with lower values (0.16-0.18 kg water/kg initial dry solid). In the case of adsorption process, hemp shiv was the sample with a stronger water bound in the monolayer followed by flax shiv and wheat whilst miscanthus and sunflower bark were the samples with the weaker water bound. Regarding X_m, it has been noticed that sunflower (bark and pith) had the higher values indicating a higher availability of active sites for water adsorption being hemp shiv, wheat and maize bark the ones with the lower values. This trend was corroborated by a_s values obtained employing Eq. (5), Table 3. This fact makes hemp shiv the sample with the lower quantity of available active sites of all studied samples but, at the same time, the one with the stronger bounded water. Moreover, K value was near to 1 which means that water molecules that are not present in the monolayer have almost the same behaviour as liquid molecules.

During desorption process all equilibrium moisture contents were higher compared to adsorption process for each sample. In general, the samples with lower values for adsorption process remained the same in the case of desorption process. However, in the case of flax shiv and miscanthus the X_m for desorption process were the highest between all samples. This fact could be related to the compositions of these materials, Table 1, which presented the lower values of ash content having, consequently, a higher proportion of other compounds that could help to retain or absorb water.

3.4. Water absorption kinetics

Experimental data of water absorption kinetics of all studied samples presented a similar behaviour, Figure 3a. At the beginning of the immersion (first 500 min) samples quickly absorb water and then an asymptotic process of water gain takes place until achieving the equilibrium (48 h). A similar kinetic was the one observed for solid loss (SL) where it was observed that the main SL during immersion takes place at the beginning of the immersion process, Figure 3b. This phenomenon explains the difference between WA_{M0} and WA_{MF} kinetics. As it can be observed, at the beginning of the immersion process samples absorbed water and leach water-soluble compounds that lead to an increasing difference between WA_{M0} and WA_{MF}. Once the equilibrium of SL is achieved and the leaching of soluble compounds becomes almost negligible the difference between WA_{M0} and WA_{MF} remains constant. Experimental data was satisfactorily modelled employing Nagy and Vas model, Eq. (9) for WA parameters (R^2>0.98). In the case of SL modelling the fitting was not satisfactory (R^2>0.83), Table 4.

Location of Table 4 and Figure 3a and 3b

Results revealed that sunflower pith was the sample with the highest water absorption capacity (35.8 kg water/kg final dry solid) far higher than the other studied samples. The range of values for the other studied samples varied from 2.3 for rice husk up to 7.1 (kg water/kg final dry solid) for maize bark. Moreover, sunflower pith and rice husk were the samples with a higher absorption rate (they reach the equilibrium water absorption capacity faster than other ones), being hemp shiv, miscanthus and sunflower pith the ones with the lower water absorption rate. This behaviour could be related to both chemical composition and porosity of bulk material. In the case of hemp shiv and miscanthus they all have the lower values of open porosity which could lead to a slower water absorption process. This is not the case of sunflower pith, the explanation in this case may be found with the higher content of lignin and the lower content of other compounds known to be hydrophilic.

Finally, Nagy and Vas model parameters related to equilibrium (SL_∞) were in accordance with the trend obtained by Van Soest method for soluble compounds. However, their values were systematically lower than those obtained by the Van Soest method. It can be explained by the fact that during water absorption experiments only water-soluble compounds are leaching from the sample and consequently determined, compared to Van Soest method where the most part of soluble compounds (not only water-soluble) are quantified. The solid loss may be related mainly to soluble compounds that are eliminated from the samples during immersion.

4. Conclusions

Nine biobased particles available on French territory with an actual or potential use in construction were studied. Their microstructure, densities, water behaviour and chemical composition was compared. The novelty of this study lies in three essential contributions. Firstly, all plant particles were characterized with exactly the same procedure and operator, which allows a fair comparison between them in order to clear out their differences. Secondly, results of particle size distribution (log-normal distribution model), water sorption isotherms (GAB model) and water absorption kinetics (Nagy and Vas model) were satisfactorily modelled using the same model for the different samples which could be useful for the prediction or estimation of these properties for future applications. Finally, the water absorption kinetics observed were found to be consistent with the chemical composition of the plant particles and the open porosity, which highlight a fair understanding of inter-dependence of particles physical properties.

Applications of the plant particle could be the use of the plant particle alone (i.e as a raw insulation) or mixed with a binder such as clay (Colinart et al., 2020) or lime, to make biobased concrete (light), wattle and daub (medium) or coating (heavy). Based on our results, it can be concluded that there are no best or worst particles, but different particles with varying degrees of difference depending on the studied property. The knowledge of such

differences between particles allows professional construction workers to select the best particle for their need, or alternatively, to adapt its practices depending on the plant particle locally available. For instance, quantity of soluble compounds might be an issue when using lime binder. Water absorption rate explains the workability or texture evolution when the particle is mixed with a binder in a mixer, or the hardening behaviour for sprayed biobased concrete. Sorption in the medium relative humidity range illustrates the water regulation capabilities of the material. From a practical point of view it is useful to evaluate if the use of a different plant particle in a biobased concrete would affect its water regulation capabilities. This study is a first step since it was carried out on only one batch for each type of plant. Further studies might be focused on the variability of each plant types in order to assess the range of dispersion for each studied characteristic. Plant diversity allows a wide range of methods in construction. Each construction applications (particle boards, lime-based mortars/renders, earth-based mixes, etc.) has its own characteristics and interactions with plant properties. The multitude of specifications echoes the diversity offered by plants. By working according to defined specifications, the diversity and complexity of plant particles become a source of potential.

CRediT authorship contribution statement

Santiago Arufe: Conceptualization; Investigation; Validation; Writing original draft, review and editing.

Arthur Hellouin de Ménibus: Conceptualization; Investigation; Validation; Writing review and editing.

Nathalie Leblanc: Investigation; Validation; Writing review and editing.

Hélène Lenormand: Conceptualization; Investigation; Validation; Writing review and editing.

Declaration of Competing Interest

The authors report no declarations of interest.

Acknowledgments

The authors acknowledge the financial support of the Normandie region and FEDER for the TIGRE research project, the Parc Naturel Régional du Perche (especially Florence Sbile), Pierre Delot for kindly providing rice husk and several information regarding such plant particles, Marianne Rosa and Jean Baptiste Besnier for additional measurements using SEM and DVS.

References

AFNOR (1997). NF V 18-122-Aliments des animaux-Détermination séquentielle des constituants pariétaux-Méthode par traitement aux détergents neutre et acide et à l'acide sulfurique.

Amziane, S., Collet, F., 2017. Based Building Materials, Vol. 23 of RILEM State-of-the-Art Reports, Springer Netherlands, Dordrecht.

Brunauer, S., Emmet, P.H., Teller E., 1938. Adsorption of gases in multimolecular layers. J. Am. Chem. Soc. 60, 309-19.

Chabriac, P.A., Gourdon, E., Glé, P., Fabbri, A., Lenormand, H., 2016. Agricultural by-products for building construction and modeling to predict micro-structural parameters. Constr. Build. Mater. 112, 158-167.

Chandrasekhar, S., Satyanarayana, K.G., Pramada, P.N., Raghavan, P., 2003. Review Processing, properties and applications of reactive silica from rice husk-an overview. J. Materials Sci. 38, 3159-3168.

Colinart, T., Vinceslas, T., Lenormand, H., Hellouin De Menibus, A., Hamard, E., Lecompte, T., 2020. Hygrothermal properties of light-earth building materials. J. Build. Eng. 29, 101134.

Collet, F., Bart, M., Serres, L., Miriel., J., 2008. Porous structure and water vapour sorption of hemp-based materials. Constr. Build. Mater. 22, 1271-1280.

Degrave-Lemeurs, M., Glé, P. Hellouin de Menibus, A., 2018. Acoustical properties of hemp concretes for buildings thermal insulation: Application to clay and lime binders. Constr. Build. Mater. 160, 462-474.

Delannoy, G., Marceau, S., Glé, P., Gourla. E, Guéguen-Minerbe, M., Diafi, D., Amziane, S., Farcas, F., 2020. Impact of hemp shiv extractives on hydration of Portland cement. Const. Buil. Mater. 244, 118300.

Diquélou, Y., Gourlay, E., Arnaud, L., Kurek, B., 2015. Impact of hemp shiv on cement setting and hardening: Influence of the extracted components from the aggregates and study of the interfaces with the inorganic matrix. Cem. Concr. Compos. 55, 112-121.

Giroudon, M., Laborel-Préneron, A., Aubert, J. E., Magniont, C., 2019. Comparison of barley and lavender straws as bioaggregates in earth bricks. Constr. Build. Mater. 202, 254-265.

Glé P., Gourlay E., 2015. Rapport de recherche MABIONAT, Étude de l'influence de la teneur en eau et du vieillissement sur les performances acoustiques et thermiques des matériaux biosourcés.

Glé, P., Lecompte, T., Hellouin de Ménibus, A., Lenormand, H., Arufe, S., Château, C., Fierro, V., Celzard, A., 2021. Densities of hemp shiv for building: From multiscale characterisation to application. Ind. Crops Prod. 164, 113390.

Honoré, M., Pimbert, S., Lecompte, T., 2020. Characterisation of plant flours for biocomposite applications focussing on *Phragmites australis* properties. Biosystems Eng. 197, 367-377.

Hussain, A., Calabria-Holley, J., Lawrence, M., Jiang, Y., 2019. Resilient hemp shiv aggregates with engineered hygroscopic properties for the building industry. Constr. Build. Mater. 212, 247-253.

Jiang, Y., Lawrence, M., Zhang, M., Cui J., 2020. Industrial bio-based plant aggregates as hygric and insulating construction materials for energy efficient building. Front. Chem. Sci. Eng.

511 Laborel-Preneron, A., Aubert, J, E. Magniont, C., Tribout, C., Bertron, A., 2016. Plant
512 aggregates and fibers in earth construction materials: A review. Constr. Build. Mater.
513 111, 719-734.
514 Lagouin, M., Magniont, C., Sénéchal, P., Moonen, P., Aubert, J.E., Laborel-Préneron, A.,
515 2019. Influence of types of binder and plant aggregates on hygrothermal and
516 mechanical properties of vegetal concretes. Const. Build. Mater. 222, 852-871.
517 Lenormand, H., Glé, P., Leblanc, N., 2017. Investigation of the acoustical and thermal
518 properties of sunflower particleboards. Acta Acust united Ac. 103, 149–157.
519 Mahieu, A., Alix, S., Leblanc, N., 2019. Properties of particleboards made of agricultural by-
520 products with a classical binder or self-bound. Ind. Crops Prod. 130. 371-379.
521 Nagy, V., Vas, L. M., 2003. Intrayarn Porosity and Pore Size in Polyester Staple Yarns. In:
522 International Textile Design and Engineering Conference Proceedings, Eninburgh,
523 United Kingdom, pp. 201-208.
524 Ntimugura, F., Vinai, R., Harper, A., Walker, P., 2020. Mechanical, thermal, hygroscopic and
525 acoustic properties of bio-aggregates – lime and alkali - activated insulating composite
526 materials: A review of current status and prospects for miscanthus as an innovative
527 resource in the South West of England. Sustainable Mat. Tech. 26, e00211.
528 Pintiaux, T., Viet, D., Vandenbossche, V., Rigal, L., and Rouilly, A. (2015). Binderless
529 materials obtained by thermo-compressive processing of lignocellulosic fibers: A
530 comprehensive review. BioRes. 10(1): 1915-1963.
531 Tayeh, B.A., Alyousef, R., Alabduljabbar, H., Alaskar, A., 2021. Recycling of rice husk waste
532 for a sustainable concrete: A critical review. J. Cleaner Prod. 312, 127734.
533 Quirijns, E.J., van Boxtel, A., van Loon, W., van Straten, G., 2005. Sorption isotherms, GAB
534 parameters and isosteric heat of sorption. J. Sci. Food Agric. 85:1805–1814.
535 van den Berg, C., Bruin, S., 1981. Water activity and its estimation in food systems:
536 theoretical aspects. In L. B. Rockland and G. F. Stewart (Eds.), pp. 1-61.

Viel, M., Collet, F., Lanos, C., 2018. Chemical and multi-physical characterization of agro-resources' by-product as a possible raw building material. Ind. Crops Prod. 120, 214-237.

Wang, L., Lenormand, H., Zmamou, H., Leblanc N., 2019. Effect of soluble components from plant aggregates on the setting of the lime-based binder. J. Renew. Mater.7, 9, 903-913.

Zhang, J., Wang,Y.H., Qu, Y.S., Wei, Q.Y., Li, H.Q., 2018. Effect of the organizational difference of corn stalk on hemicellulose extraction and enzymatic hydrolysis. Ind. Crops Prod. 112, 698-704.

Caption for Figures

Figure 1. Images of the studied plant particles. A: Flax Shiv; B: Hemp Shiv; C: Maize Bark; D: Miscanthus; E: Reed; F: Rice Husk; G: Sunflower Bark; H: Sunflower Pith; I: Wheat.

Figure 2. Water adsorption (A) and desorption (B) isotherms of the studied systems. Line corresponds to GAB model, Eq. (3).

Figure 3. Water absorption (A) and solid loss kinetics (B) of the studied systems. Line corresponds to Nagy and Vas model, Eq. (9).

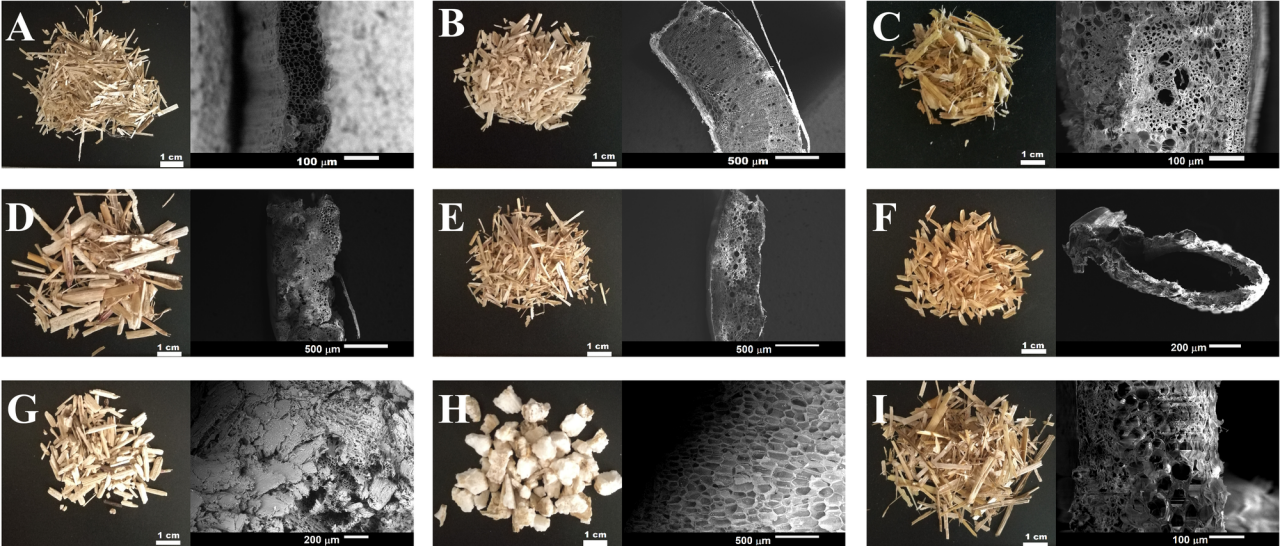
A
1 cm
100 μm
B
1 cm
500 μm
C
1 cm
100 μm
D
1 cm
500 μm
E
1 cm
500 μm
F
1 cm
200 μm
G
1 cm
200 μm
H
1 cm
500 μm
I
1 cm
100 μm

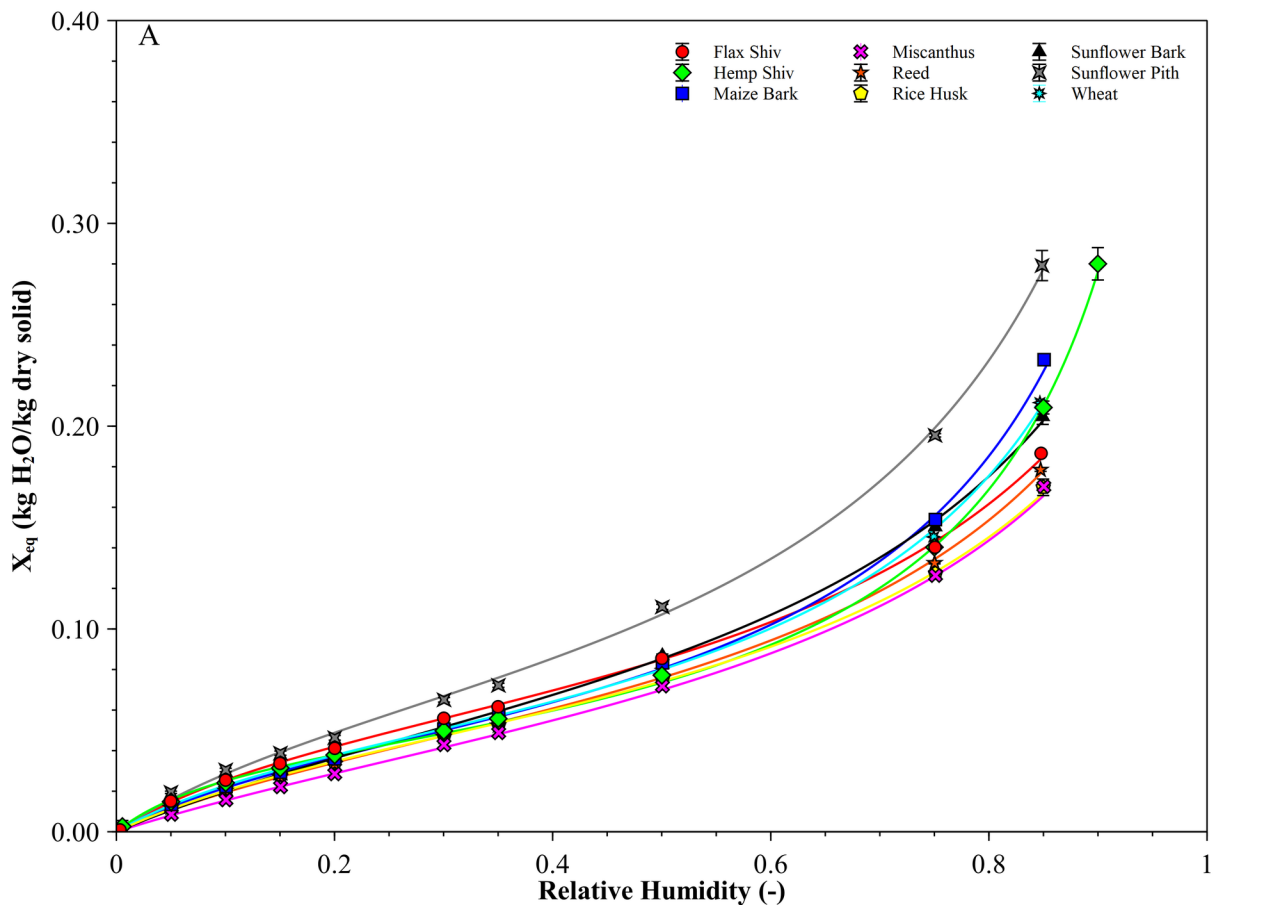
A
Flax Shiv
Hemp Shiv
Maize Bark
Miscanthus
Reed
Rice Husk
Sunflower Bark
Sunflower Pith
Wheat
0.40
0.30
0.20
0.10
0.00
0
0.2
0.4
0.6
0.8
1
Xeq (kg H2O/kg dry solid)
Relative Humidity (-)

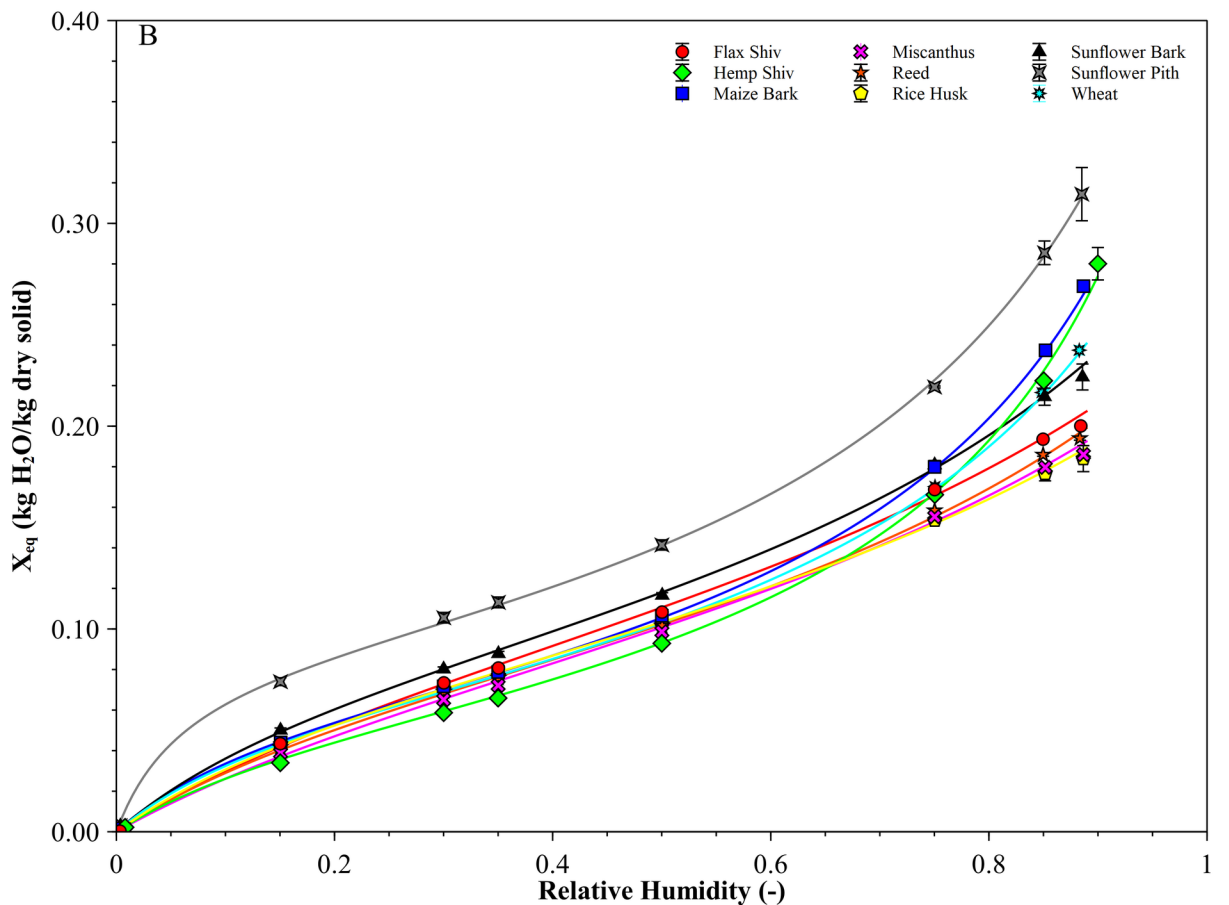
B
Flax Shiv
Hemp Shiv
Maize Bark
Miscanthus
Reed
Rice Husk
Sunflower Bark
Sunflower Pith
Wheat
0.40
0.30
0.20
0.10
0.00
X_{eq} (kg H_2O/kg dry solid)
0
0.2
0.4
0.6
0.8
1
Relative Humidity (-)

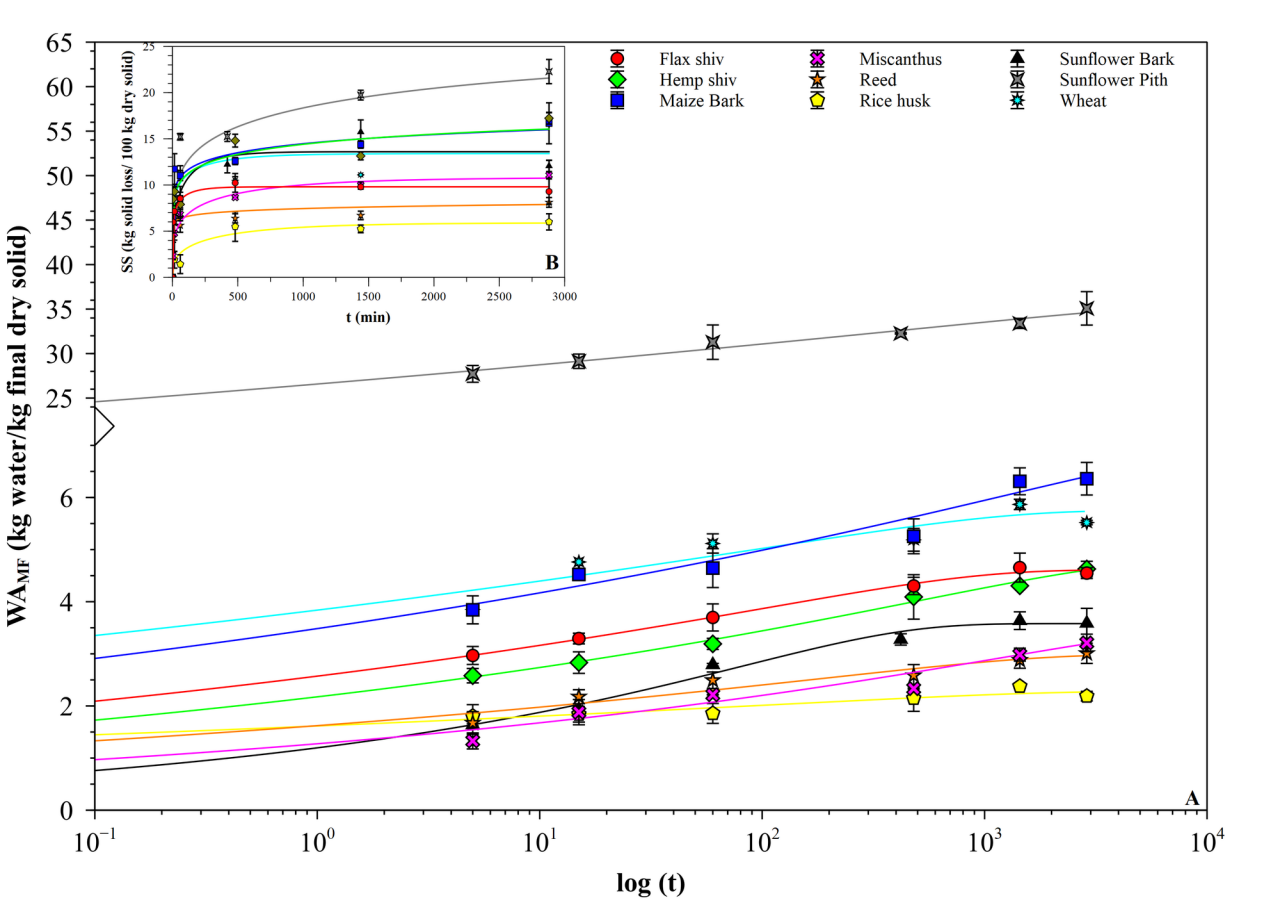
Flax shiv
Hemp shiv
Maize Bark
Miscanthus
Reed
Rice husk
Sunflower Bark
Sunflower Pith
Wheat
WA_MF (kg water/kg final dry solid)
log (t)
A
SS (kg solid loss/ 100 kg dry solid)
t (min)
B

Table 1. Chemical composition of different studied plant particles.

Sample	Soluble (% d.b.)	Hemicellulose (% d.b.)	Cellulose (% d.b.)	Lignin (% d.b.)	Ash (% d.b.)	$X_{initial}$ (% d.b.)
Flax Shiv	9.1±1.9	17.6±2.4	43.5±4.7	27.1±4.5	2.7±0.9	4.7±0.7
Hemp Shiv	17.2±1.1	21.6±1.8	49.0±2.8	8.1±0.6	4.1±1.6	3.1±0.4
Maize Bark	15.3±0.2	34.8±0.9	42.8±1.0	3.3±0.2	3.8±0.2	2.8±0.1
Miscanthus	7.2±0.5	27.8±1.4	43.6±9.8	19.0±10.8	2.4±0.1	3.5±1.5
Reed	9.6±1.5	28.3±1.3	47.6±1.2	10.5±1.5	4.0±0.1	2.4±0.1
Rice Husk	7.7±0.3	19.8±0.5	42.1±0.6	16.8±0.2	13.7±0.1	1.9±0.1
Sunflower Bark	6.0±2.2	18.1±2.8	30.3±6.2	41.7±8.5	3.8±0.5	6.5±0.1
Sunflower Pith	38.6±1.1	5.0±1.9	23.3±6.8	21.4±6.4	11.7±0.3	8.7±0.3
Wheat	10.5±0.1	34.1±4.5	45.3±4.3	6.2±0.3	3.9±0.1	5.5±0.1

% d.b.: g/100 g dry solid; $X_{initial}$: Humidity of samples before starting the tests.

Table 2. Parameters of Lognormal function, Eq. (1), corresponding to systems length and width frequency distribution, apparent (ρ_A), compacted (ρ_C) and true (ρ_T) densities and open porosity ($\theta=1-\rho_A/\rho_T$), Eq. (2).

	Length				Width				Density (kg/m^3)			Open Porosity (-)
Sample	**μ**	**σ**	**R^2**	**E_{RMS} (-)**	**μ**	**σ**	**R^2**	**E_{RMS} (-)**	**ρ_B**	**ρ_C**	**ρ_T**	**θ**
Flax Shiv	2.070	0.320	0.999	0.008	0.265	0.330	0.999	0.009	101±5	144±4	1406±19	0.928
Hemp Shiv	1.503	0.546	0.999	0.011	0.157	0.565	0.998	0.013	114±4	167±6	1247±41	0.909
Maize Bark	1.633	0.633	0.999	0.010	0.446	0.760	0.999	0.008	67±2	112±3	1075±6	0.938
Miscanthus	1.812	0.829	0.998	0.014	0.288	1.036	0.997	0.015	128±5	186±9	940±9	0.864
Reed	2.057	0.679	0.998	0.017	0.283	0.639	0.997	0.010	81±2	134±3	1016±11	0.920
Rice Husk	2.077	0.129	0.985	0.040	0.840	0.305	0.997	0.015	112±2	147±4	1328±26	0.916
Sunflower Bark	2.373	0.385	0.997	0.017	1.364	0.330	0.999	0.010	157±9	176±6	1395±12	0.887
Sunflower Pith	1.641	0.395	0.998	0.014	1.278	0.400	0.999	0.009	21±3	31±4	754±25	0.973
Wheat	2.233	0.596	0.999	0.011	0.557	0.731	0.993	0.027	45±4	85±5	1163±13	0.961

Table 3. GAB model, (Eq. 3), parameters for water sorption isotherms of studied plant particles.

Agroresource	Adsorption					Desorption					a_s (m^2/g)
	C (-)	K (-)	X_m (d.b.)	R^2 (-)	E_{RMS} (d.b.)	C (-)	K (-)	X_m (d.b.)	R^2 (-)	E_{RMS} (d.b.)	Eq. (5)
Flax Shiv	7.0±0.1	0.812±0.004	0.061±0.001	0.9995	0.002	5.2±0.4	0.607±0.038	0.111±0.010	0.9994	0.003	178.9±0.6
Hemp Shiv	10.8±1.3	0.941±0.008	0.043±0.001	0.9997	0.002	6.3±1.3	0.863±0.034	0.064±0.007	0.9997	0.002	156.6±8.0
Maize Bark	6.0±0.2	0.919±0.006	0.052±0.001	0.9998	0.002	8.2±0.4	0.834±0.010	0.072±0.002	0.9999	0.001	168.8±0.1
Miscanthus	3.6±0.1	0.805±0.001	0.060±0.001	0.9996	0.002	4.8±0.4	0.612±0.031	0.103±0.008	0.9994	0.003	170.1±1.8
Reed	5.0±0.1	0.829±0.001	0.057±0.001	0.9997	0.001	5.9±0.1	0.660±0.013	0.092±0.002	0.9997	0.002	158.2±1.1
Rice Husk	5.7±0.2	0.817±0.015	0.055±0.001	0.9997	0.001	6.5±0.1	0.618±0.023	0.096±0.003	0.9997	0.002	172.3±2.4
Sunflower Bark	4.1±0.1	0.820±0.009	0.068±0.001	0.9997	0.002	7.0±0.1	0.684±0.003	0.099±0.001	0.9997	0.002	196.9±5.8
Sunflower Pith	5.7±0.1	0.884±0.018	0.073±0.003	0.9997	0.002	20.2±1.1	0.811±0.030	0.090±0.005	0.9998	0.002	205.2±1.6
Wheat	6.7±0.2	0.900±0.002	0.052±0.001	0.9998	0.001	7.8±0.2	0.796±0.004	0.074±0.000	0.9999	0.000	160.8±0.1

d.b.: g water/g dry solid

Table 4. Nagy and Vas model parameter, Eq. (9), for different plant particles.

Parameter	Flax shiv	Hemp shiv	Maize Bark	Miscanthus	Reed	Rice Husk	Sunflower Bark	Sunflower Pith	Wheat
$WA_{F\infty}$ (kg water/ kg d.s.)	4.6	4.8	7.1	3.6	3.0	2.3	3.6	35.8	5.7
A_{WAF}	0.033	0.007	0.003	0.003	0.019	0.032	0.039	0.009	0.036
K_{WAF}	0.089	0.100	0.078	0.119	0.086	0.048	0.197	0.034	0.059
R^2	0.999	0.998	0.991	0.976	0.983	0.989	0.993	0.999	0.983
E_{RMS} (kg water/ kg f.d.s.)	0.1	0.1	0.2	0.2	0.1	0.1	0.1	0.4	0.2
$WA_{0\infty}$ (kg water/ kg i.d.s.)	4.1	3.7	5.8	3.1	2.6	2.1	3.0	29.0	4.9
A_{WA0}	0.027	0.035	0.003	0.003	0.170	0.055	0.051	0.009	0.057
K_{WA0}	0.078	0.110	0.065	0.112	0.187	0.036	0.182	0.012	0.050
R^2	0.999	0.998	0.992	0.982	0.986	0.991	0.988	1.000	0.979
E_{RMS} (kg water/ kg i.d.s.)	0.0	0.1	0.1	0.1	0.1	0.1	0.1	0.4	0.2
SL_{∞}(kg solid/ kg i.d.s.)	9.8	17.9	18.4	10.8	9.1	5.9	13.6	25.4	13.4
A_{SL}	0.124	0.003	0.002	0.011	0.001	0.009	0.034	0.002	0.038
K_{SL}	0.162	0.121	0.104	0.229	0.056	0.332	0.287	0.181	0.143
R^2	0.994	0.927	0.941	0.975	0.960	0.918	0.868	0.940	0.838
E_{RMS} (kg solid/ kg i.d.s.)	0.3	1.4	1.3	0.6	0.5	0.6	1.9	1.9	2.0

kg i.d.s.: kg of initial dry solid; kg f.d.s.: kg of final dry solid